A thermal-based remote sensing technique for routine mapping of land-surface carbon, water and energy fluxes from field to regional scales

M.C. Anderson [a,*], J.M. Norman [b], W.P. Kustas [a], R. Houborg [a], P.J. Starks [c], N. Agam [a]

[a] USDA-ARS, Hydrology and Remote Sensing Lab, Bldg. 007, BARC-West, Beltsville, MD 20705, United States
[b] Department of Soil Science, University of Wisconsin, Madison, WI, 53706, United States
[c] USDA-ARS, Grazinglands Research Laboratory, El Reno, OK 73036, United States

ARTICLE INFO

ABSTRACT

Robust yet simple remote sensing methodologies for mapping instantaneous land-surface fluxes of water, energy and CO_2 exchange within a coupled framework add significant value to large-scale monitoring networks like FLUXNET, facilitating upscaling of tower flux observations to address questions of regional carbon cycling and water availability. This study investigates the implementation of an analytical, light-use efficiency (LUE) based model of canopy resistance within a Two-Source Energy Balance (TSEB) scheme driven primarily by thermal remote sensing inputs. The LUE model computes coupled canopy-scale carbon assimilation and transpiration fluxes, and replaces a Priestley–Taylor (PT) based transpiration estimate used in the original form of the TSEB model. In turn, the thermal remote sensing data provide valuable diagnostic information about the sub-surface moisture status, obviating the need for precipitation input data and prognostic modeling of the soil water balance. Both the LUE and PT forms of the model are compared with eddy covariance tower measurements acquired in rangeland near El Reno, OK. The LUE method resulted in improved partitioning of the surface energy budget, capturing effects of midday stomatal closure in response to increased vapor pressure deficit and reducing errors in half-hourly flux predictions from 16 to 12%. The spatial distribution of CO_2 flux was mapped over the El Reno study area using data from an airborne thermal imaging system and compared to fluxes measured by an aircraft flying a transect over rangeland, riparian areas, and harvested winter wheat. Soil respiration contributions to the net carbon flux were modeled spatially using remotely sensed estimates of soil surface temperature, soil moisture, and leaf area index. Modeled carbon and water fluxes from this heterogeneous landscape compared well in magnitude and spatial pattern to the aircraft fluxes. The thermal inputs proved to be valuable in modifying the effective LUE from a nominal species-dependent value. The model associates cooler canopy temperatures with enhanced transpiration, indicating higher canopy conductance and carbon assimilation rates. The surface energy balance constraint in this modeling approach provides a useful and physically intuitive mechanism for incorporating subtle signatures of soil moisture deficiencies and reduced stomatal aperture, manifest in the thermal band signal, into the coupled carbon and water flux estimates.

Published by Elsevier Inc.

1. Introduction

Given the physical interconnections between the land-surface water, energy and carbon cycles, and the importance of understanding and quantifying these cycles as they apply to issues of climate change and water availability, there is benefit to developing robust yet simple remote sensing models that will simulate regional fluxes of latent and sensible heat and CO_2 exchange within a unified, self-consistent framework. Remote sensing models provide the spatial context for upscaling point flux measurements from large-scale tower networks like FLUXNET to assessments of the carbon and water budgets at the continental scale. In the remote sensing community, models of evapotranspiration and carbon flux have tended to evolve independently, using very different physical constraints and modeling approaches (e.g., energy balance vs. biogeochemical cycling). However, because CO_2 and water exchanges at the leaf surface are jointly controlled by stomatal aperture, these fluxes can be well correlated in space and time at the landscape scale and such natural correlations are best reproduced by a coupled modeling approach. Furthermore, the additional constraints required to model the bulk canopy resistance and assimilation flux have the potential for improving estimates of ET from surface energy balance models, provided the required meteorological inputs and model parameters can be specified with adequate accuracy.

The benefits of coupled modeling systems have been realized in many studies at the plant to canopy scales where biochemical models

of photosynthesis (Farquhar et al., 1980; Berry and Farquhar, 1978; Collatz et al., 1992) and models of stomatal resistance (Jarvis, 1976; Wong et al., 1979; Ball et al., 1986; Leuning, 1990, 1995) have been embedded within a surface energy and water balance framework (e.g., Norman, 1979; Leuning et al., 1995; Sellers et al., 1996; Baldocchi and Wilson, 2001; Kim and Lieth, 2003; Tuzet et al., 2003). The energy balance component is critical as it determines the characteristic leaf temperature, which in turn influences vapor pressure gradients and relative humidity conditions at the leaf surface governing transpiration and stomatal resistance, and the kinetics of carbon uptake. Soil water potential influences stomatal aperture (Gollan et al., 1986), and so a functional description of water supply from the plant root zone is also important (Tuzet et al., 2003). Increased stomatal resistance reduces transpiration water losses and evaporative cooling of the leaf surface, thereby increasing leaf temperature, so exchanges of water, heat and carbon are intimately coupled.

While deterministic, bottom–up modeling approaches allow detailed examination of important canopy-scale processes, they can be difficult to apply at the regional scale because they require accurate specification of numerous soil and plant physiological characteristics and parameter values. A sub-surface soil water balance must be maintained at each model grid cell, along with species-appropriate root uptake functions connecting the soil and plant water potentials. Biases in input fields describing antecedent precipitation rates and soil hydraulic properties can lead to significant biases in the modeled fluxes that will accumulate with time (Betts et al., 1997; Schaake et al., 2004). In addition, mechanistic models of carbon fixation developed at the leaf scale require robust schemes for upscaling to the canopy and regional levels. Complex feedback systems can cause bulk stomatal response to external driving factors to be highly scale dependent (McNaughton and Jarvis, 1991; Avissar, 1993; Anderson et al., 2003).

These data and modeling demands can be relieved to some extent by using remote sensing to diagnose important surface conditions, bypassing the need to model these conditions explicitly. Zhan and Kustas (2001), for example, describe a diagnostic method for modeling coupled CO_2 and water vapor fluxes that uses remote sensing information in the thermal infrared (TIR) band in place of a soil moisture submodel. Thermal imaging can detect elevated canopy temperatures resulting from moisture deficits in the plant root zone and, in partially vegetated landscapes, the increase in soil surface temperature as the surface available moisture is depleted (e.g., Smith et al., 1985; Gillies and Carlson, 1995; Moran, 2003; Anderson et al., 2007a). Zhan and Kustas (2001) incorporated models of photosynthesis and stomatal resistance into the Two-Source (soil+canopy) Energy Balance (TSEB) model (Norman et al., 1995), which partitions surface radiometric temperature into component soil and canopy temperatures. These component temperatures effectively integrate effects of both the sub-surface moisture status and the radiative/ meteorological forcings on the system. Zhan and Kustas found that the radiometric temperature data were an effective substitute for in-situ surface moisture observations, and in fact gave better agreement with observed fluxes than did a model version using soil moisture data directly. TIR remote sensing data have also been used in a data assimilation mode to recalibrate temperature and moisture-related parameters in ET-photosynthesis models (Olioso et al., 1999; Coudert and Ottlé, 2007; Coudert et al., 2008).

Monteith (1966) suggested that the photosynthesis component of coupled modeling systems might be simplified by using measurements of canopy light-use efficiency (LUE, also designated β). Here, LUE is defined as the ratio between net canopy carbon assimilation rate, A_C, and the photosynthetically active radiation (PAR) absorbed by the vegetative canopy (APAR). LUE models provide an economical means for mapping carbon exchange over large geographical regions because they require relatively few species-dependent parameters and are founded on APAR, a quantity that can be derived with

reasonable accuracy from remote sensing (e.g., Myneni et al., 1995; Landsberg et al., 1997). Light-use efficiency has been found to be fairly conservative within broad plant species when the vegetation is unstressed and when disparities in measurement technique are accounted for (Monteith, 1977; Arkebauer et al., 1994; Goetz and Prince, 1998; Gower et al., 1999; Anderson et al., 2000), with extensive data for many species available in the literature. And because assimilation scaling effects are implicitly incorporated into stand-level measurements of LUE, β can provide a valuable constraint to carbon flux modeling at the regional scale.

Prominent LUE models of net primary production include BIOME-BGC (Running and Hunt, 1993) and the CASA (Carnegie Ames Stanford Approach) model (Potter et al., 2003), which are process based, running on daily to monthly timesteps. These biogeochemical models track the stocks and transfer of carbon in and between various pools, accounting for litter fall, decomposition, soil nutrient mineralization, and CO_2 exchange with the atmosphere. Moisture stress functionals modifying a nominal unstressed LUE are typically derived using observed or simulated precipitation data and a soil moisture storage model, while temperature stress is inferred from gridded air temperatures.

Anderson et al. (2000) proposed an alternative, micrometeorological approach for implementing a LUE constraint on CO_2 exchanges. This approach employs an analytical expression for the bulk canopy resistance that is semi-constrained by a nominal value of unstressed canopy LUE. Coupled canopy transpiration and carbon assimilation fluxes are computed using gradient-resistance equations, which can be evaluated at sub-hourly timesteps. Anderson et al. (2000) demonstrated that when embedded within a prognostic modeling framework using boundary conditions supplied by numerical soil heat and water transport sub-models and in-situ weather measurements, the analytical canopy resistance model accurately reproduced micrometeorological measurements of water, energy and carbon fluxes acquired over forest, grassland, and agricultural sites.

In this paper, we evaluate the performance of the analytical canopy resistance model when embedded within the diagnostic thermal-based TSEB model. The result is a fully coupled carbon–water–energy balance model based on remote sensing that is well suited for routine regional applications. This model can be applied to thermal imagery from geostationary satellites like GOES (5–10 km) or polar orbiting satellites like Landsat (60–120 m resolution), ASTER (90 m), MODIS (1 km) or from aircraft (<50 m), and so presents a flexible and scalable mechanism for generating surface flux distributions that may be useful in reconciling "top–down" (e.g., atmospheric) and "bottom–up" (e.g., scaled leaf) flux modeling and measurement strategies, with the goal of improving regional scale carbon and water budgets.

The coupled modeling system is evaluated using tower and aircraft flux measurements collected over the El Reno (ER) study area during the Southern Great Plains experiment of 1997 (SGP97; Jackson et al., 1999), a heterogeneous landscape with strong variability in vegetation cover and moisture conditions. The value of the thermal remote sensing inputs in the carbon flux assessment is reflected in the fact that the modeled effective LUE adjusts from the nominal value in response to variability in surface temperature across the landscape, enhancing canopy carbon uptake in areas where cooler canopy temperatures suggest higher values of transpiration and canopy conductance.

Section 2 provides a description of the original form of the TSEB model (TSEB_PT), which uses the Priestley–Taylor (PT) approximation (Priestley and Taylor, 1972) to obtain an initial estimate of canopy transpiration and has been previously evaluated over the ER study area using both local and regional forcings (Norman et al., 2003; French et al., 2003; Kustas et al., 2006). LUE-based modifications to the TSEB (TSEB_LUE) are then outlined, along with a simple soil respiration model geared towards remote sensing. The hierarchical data collection scheme used in SGP97 is described in Section 3,
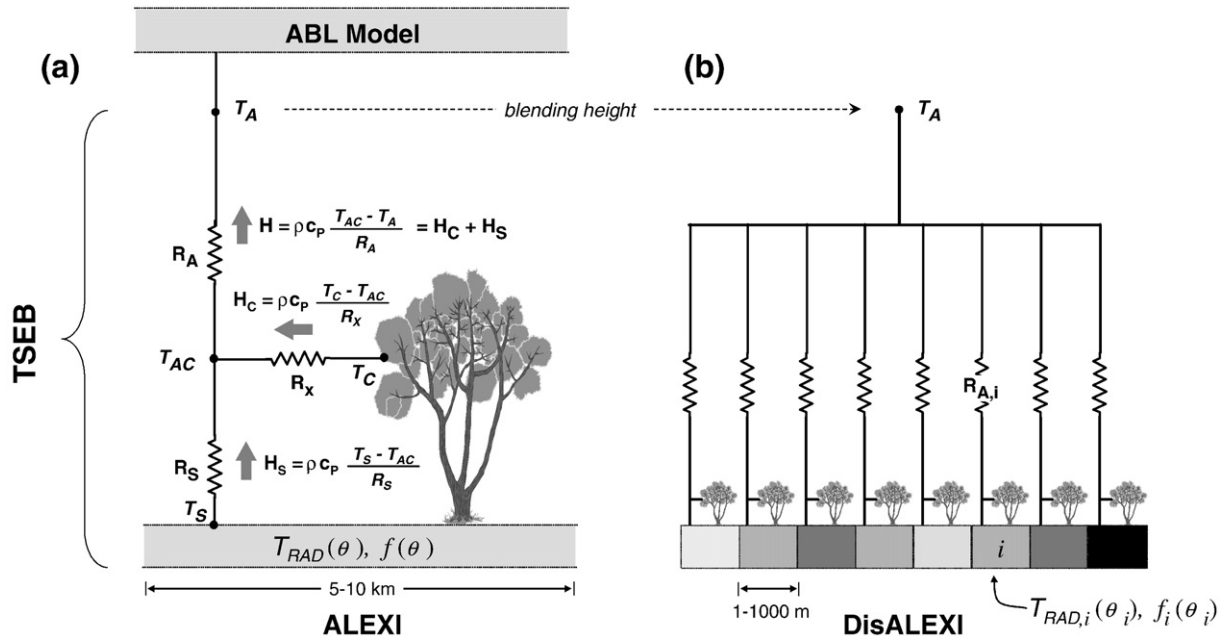
Fig. 1. Schematic diagram representing the ALEXI (a) and DisALEXI (b) modeling schemes, highlighting fluxes of sensible heat (*H*) from the soil and canopy (subscripts 's' and 'c') along gradients in temperature (*T*), and regulated by transport resistances R_A (aerodynamic), R_x (bulk leaf boundary layer) and R_S (soil surface boundary layer). DisALEXI uses the air temperature predicted by ALEXI near the blending height (T_A) to disaggregate 5–10 km ALEXI fluxes, given vegetation cover ($f(\theta)$) and directional surface radiometric temperature ($T_{RAD}(\theta)$) information derived from high-resolution remote sensing imagery at look angle θ. See Norman et al. (2003) for further details.

combining local observations at distributed tower sites with regional flux and remote sensing from aircraft overflights to upscale fluxes to the watershed level. In Section 4, the relative utility of the TSEB_PT and TSEB_LUE models is compared in terms of energy budget partitioning, using TIR and micrometeorological data collected at two tower sites in the ER study area. An application of the regional TSEB_LUE model to aircraft remote sensing in TIR, shortwave and microwave bands is described in Section 5, with comparisons against spatial patterns in fluxes measured over the aircraft transect. Finally, prospects for further model development and applications are outlined in Section 6.

2. Model description

2.1. TSEB-DisALEXI

The modeling system proposed here is based on the series version of the diagnostic Two-Source Energy Balance (TSEB) land-surface representation of Norman et al. (1995), and subsequent modifications described by Kustas and Norman (1999b, 2000). The TSEB partitions the observed directional surface radiometric temperature, $T_{RAD}(\theta)$, into soil and canopy temperature components, T_S and T_C, based on the local green vegetation cover fraction apparent at the thermal sensor view angle, $f(\theta)$:

$$T_{RAD}(\theta) = \left[f(\theta)T_C^4 + [1-f(\theta)]T_S^4 \right]^{1/4},$$ (1)

along with equations governing energy balance in the soil and canopy subsystems. For a homogeneous canopy with a spherical leaf angle distribution and leaf area index (LAI) *F*,

$$f(\theta) = 1 - \exp\left(\frac{-0.5F}{\cos\theta}\right).$$ (2)

Sensible heat fluxes from the soil and canopy (H_S and H_C) are directly constrained by the derived soil and canopy temperatures and a measurement or estimate of above-canopy air temperature (T_A; see Fig. 1). Given these fluxes and remotely sensed estimates of soil and

canopy net radiation (RN$_S$ and RN$_C$), soil heat conduction (*G*), and canopy transpiration (LE$_C$), the evaporation from the soil surface (LE$_S$) is computed as a residual to the two-source surface energy balance equation:

$$LE_S = RN_C + RN_S - G - H_S - H_C - LE_C.$$ (3)

Two alternative methods for estimating LE$_C$ are described and compared below, and input data requirements for regional application of the TSEB are listed in Table 1. The basic equation set is outlined in Table A1.

For mapping over field campaign sites, the upper boundary conditions in air temperature required for the TSEB have typically been obtained from a meteorological station located within the modeling scene (Kustas et al., 2004; Li et al., 2006, 2008). In general, however, we cannot rely on the availability of local air temperature data, and interpolated temperatures from synoptic datasets generally do not have adequate accuracy and consistency with the TIR data for good flux assessments. Therefore, for regional scale flux mapping, the

Table 1
Primary input data used in the TSEB_PT and TSEB_LUE models, and data sources for regional application (DisALEXI) over the ER study area

Data	Purpose	Source
PT and LUE		
T_{RAD}	Surface temperature	TIMS
T_A	Upper boundary	ALEXI
LAI	TSEB partitioning, roughness	TMS
Land-cover type	Assigning parameter values	TMS
Downwelling radiation	Net radiation	GOES
Windspeed	Transport resistances	Synoptic[a]
LUE only		
e_A	Upper boundary	Synoptic[a]
C_A	Upper boundary	Climatology

[a] Meteorological data from the standard U.S. synoptic weather network (~100-km spacing) been analyzed to 40-km resolution within the analysis component of the Cooperative Institute for Meteorological Satellite Studies (CIMSS) mesoscale model (Diak et al., 2003).

TSEB has been coupled with a simple model of atmospheric boundary layer (ABL) development (McNaughton & Spriggs, 1986) such that above-canopy air temperature is simulated internally at a nominal blending height and is consistent with the modeled surface fluxes (Anderson et al., 1997; see Fig. 1). The primary remote sensing input to the resulting Atmosphere-Land Exchange Inverse (ALEXI) model is a measurement of morning surface temperature rise, which can be obtained in the U.S. with the Geostationary Operational Environmental Satellites (GOES). Currently, the regional ALEXI model is being applied on a daily basis at 10-km resolution over the continental U.S. using data from GOES-E and -W (Anderson et al., 2007a,b), processed with an automated system. To create flux maps at finer resolutions than those afforded by geostationary satellites, Norman et al. (2003) developed the DisALEXI technique for spatially disaggregating coarse-scale ALEXI flux estimates. The DisALEXI model is identical to the TSEB, but uses air temperatures diagnosed by ALEXI rather than local observations to evaluate fluxes at the landscape scale. While ALEXI requires time-differential temperature data, DisALEXI can be applied to single thermal images and therefore is well suited for high-resolution imaging systems on aircraft or polar orbiting satellites like Landsat, ASTER, or MODIS.

The hierarchical connections between the TSEB, ALEXI and DisALEXI models are described in greater detail by Anderson et al. (2004, 2007).

2.2. PT transpiration submodel

To estimate canopy transpiration, LE_C, the original TSEB model formulation (TSEB_PT; Norman et al., 1995) initially assigns a potential rate obtained by applying the Priestley–Taylor (PT; Priestley & Taylor, 1972) equation to the divergence of net radiation within the canopy (Tanner & Jury, 1976; see also Eq. (A10) in the Appendix A). When the observed surface temperature is higher than expected for an unstressed canopy of a given vegetation cover fraction, the energy balance algorithm causes LE_S to become negative, suggesting condensation on the soil. As this is unlikely under the midday conditions

when thermal satellite imagery are typically collected, negative LE_S is regarded as an indication that transpiration has been throttled back due to stress-induced stomatal closure, and the effective PT coefficient is therefore iteratively reduced until LE_S approaches zero.

While the PT approximation is known to have limitations (e.g., McAneney and Itier, 1996), this modeling scheme has been demonstrated to provide reasonable estimates of system latent heating over a wide range of climatic and vegetation cover conditions (Norman et al., 1995, 2003; Anderson et al., 2004; Kustas et al., 2004; Li et al., 2006, 2008). One criticism of the PT method is that the bulk coefficient, as applied to the system evapotranspiration flux, is not conservative but tends to decrease at low values of leaf area index (LAI). This is an artifact of the fact that ET at low cover is dominated by direct soil evaporation, which diminishes rapidly after a rainfall event (Stannard, 1993).

Still, the PT approximation may be limiting the accuracy of TSEB_PT partitioning of LE between LE_C and LE_S under some conditions. First, there is no trigger for downadjusting the canopy PT coefficient until the $LE_S = 0$ threshold is reached. This may result in an overestimation of LE_C under conditions of moderate, midday stomatal closure. Similarly, there is no built-in mechanism in TSEB_PT for increasing the PT coefficient in response to enhanced atmospheric demand, as in areas of high vapor deficit and strong dry air advection. Kustas and Norman (1999a) found that in irrigated row cotton in Arizona, the canopy PT coefficient had to be increased a priori from a typical value of 1.26 to 2.0 to account for increased local evaporation due to advection of hot dry air from surrounding areas of unirrigated and uncultivated bare soil. Both of these situations may be better addressed under the LUE model formulation, which facilitates response to local vapor pressure conditions.

2.3. LUE transpiration/assimilation submodel

In comparison with TSEB_PT, the TSEB_LUE model (Fig. 2) requires two additional model inputs: the ambient vapor pressure (e_A) and CO_2 concentration (C_A, see Table 1); but enables the estimation of the
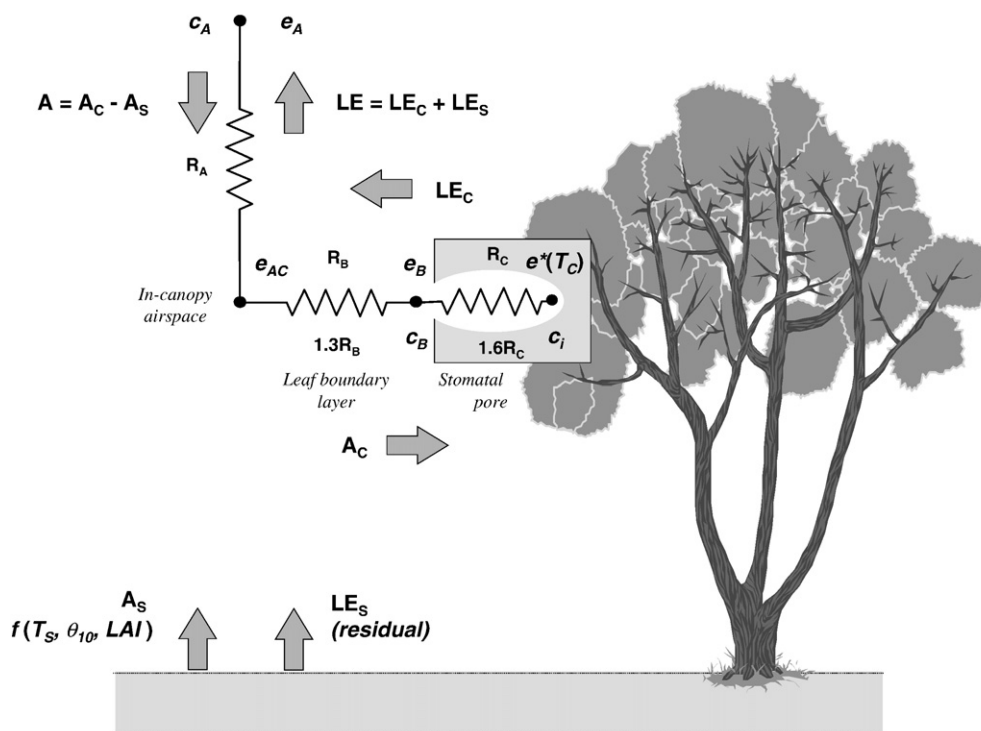

Fig. 2. Schematic diagram describing the LUE-based canopy resistance method for computing coupled carbon and water fluxes within the TSEB framework.

canopy carbon assimilation flux, which is coupled to the transpiration flux through the bulk canopy resistance (R_C). These additional inputs serve as upper boundaries for the flux-gradient computations of LE_C and A_C. The vapor pressure is particularly important for modeling stomatal response to atmospheric conditions, and enables simulation of midday stomatal closure as the in-canopy airspace becomes increasingly desiccating.

The equations describing the analytical canopy resistance model are given in Anderson et al. (2000) and summarized in Table A1. In the context of the TSEB, these equations are solved iteratively in parallel with those for the other flux components as described in Appendix A of Norman et al. (1995). The first iteration uses the PT submodel to generate initial estimates of the system latent heat flux and canopy temperature. On the 2nd iteration, the initial LE is inverted to extrapolate the vapor pressure gradient from above-canopy (e_A) to in-canopy (e_{AC}) conditions (Fig. 2). Values for e_{AC} and T_C from the TSEB are passed into the LUE submodel; together they define the water vapor pressure gradient from the substomatal cavities in the leaves (assumed to be saturated at temperature T_C; $e*(T_C)$) to the in-canopy airspace. These inputs are used along with a nominal value of LUE (β_n) and estimates of the bulk leaf boundary layer resistance, R_B, and the aerodynamic resistance, R_a, to solve a cubic function in R_C (Eq. (11) in Anderson et al., 2000). Updated estimates of LE_C (and A_C) are then obtained from R_C; then H_C, H_S and LE_S, along with T_S and T_C, are recomputed through the TSEB energy balance; and the iteration continues until the system converges using canopy temperature and sensible heat as convergence tracers.

In this process, an effective LUE (β) is diagnosed by the analytical model (Eq. (A21)). This effective LUE is modified from the nominal stand-level value (β_n; an input parameter, indexed by vegetation class), and includes response to varying environmental conditions in humidity, temperature (ambient and leaf), wind speed, CO_2 concentration, and direct beam vs. diffuse light composition through the system of micrometeorological flux-gradient equations. The change in LUE from its nominal value, $\Delta\beta = \beta - \beta_n$, reflects the magnitude of this response. In the TSEB_LUE, the canopy temperature diagnosed from the thermal remote sensing data replaces the need for a soil model and precipitation data in conveying information about the surface moisture status. All LUE model parameter values (Table A3) are derived from physical measurements reported in the literature or from simulations with a comprehensive numerical soil–plant–atmosphere model (Cupid; Norman, 1979) applied to generic datasets. No local calibration is required by either TSEB_PT or TSEB_LUE.

2.4. Soil respiration model

To compare TSEB_LUE estimates of canopy carbon assimilation (A_C) with measurements of Net Ecosystem Exchange (NEE or $A = A_C - A_S$) made by towers or aircraft, a model estimate of heterotrophic soil respiration (A_S; defined as positive away from the soil surface, as in Fig. 2) is required. In keeping with the pragmatic carbon mapping approach proposed here, we use a simple empirical model of Norman et al. (1992) that can be computed using quantities derived from remote sensing:

$$A_S = (0.135 + 0.054F)\theta_{10}\exp\left[0.069(T_{s,10} - 25.0)\right] \tag{4}$$

where F is the leaf area index (serving as a proxy indicator for root biomass), θ_{10} is the 0- to 10-cm average volumetric water content in percent, and $T_{S,10}$ is the 10-cm soil temperature (C). The coefficients in Eq. (4) were obtained using ground-based data collected during the First ISLSCP (International Satellite Land Surface Climatology Project) Field Experiment of 1987 (FIFE; Sellers et al., 1992), conducted near the Konza Prairie Research Natural Area near Manhattan, Kansas. For spatial mapping applications, soil moisture can be estimated from microwave remote sensing, LAI from a visible/near-infrared band

vegetation index like the Normalized Difference Vegetation Index (NDVI) or reflectance model inversion, while soil temperature is derived internally by the TSEB from thermal band imagery.

3. Data

3.1. Study site

Aircraft remote sensing and flux data were collected periodically over a study area near El Reno, OK (ER) during the SGP97 field experiment in July of 1997 (Fig. 3). In addition, several eddy covariance towers were deployed on the grounds of the USDA Agricultural Research Service (ARS) Grazinglands Research Laboratory, measuring time-continuous flux and micrometeorological data. The ER landscape consists primarily of rangeland and pasture, narrow forested riparian areas, and fields of winter wheat and other crops. The rangeland/pasture is a mixture of predominantly C4 (warm-season) grasses with a smaller percentage of C3 (cool-season) weeds. C4 species are typically more tolerant to high temperature and drought conditions and exhibit higher light-use efficiency, fixing more units of carbon per unit water loss than do C3 plants.

At the time of data acquisition, the pastures and rangeland were in full vegetation cover (redder areas in Fig. 3), while the winter wheat fields were generally mature and senesced or recently harvested, either with stubble or tilled to bare soil. The aircraft data analyzed here were collected on DOY 183 (2 July), 4 days into a local dry-down following a 6-cm precipitation event on DOY 179. By DOY 183, the harvested wheat fields were relatively dry whereas the grasslands and riparian areas maintained high ET rates, yielding a variable patchwork of moisture conditions across the modeling domain.

The experiment plan for SGP97 and descriptions of the sampling protocols can be found on the web at http://daac.gsfc.nasa.gov/fieldexp/SGP97/.

3.2. Aircraft flux data

Aircraft flux and atmospheric boundary layer profiling observations were made over the ER site by the National Research Council (NRC) Canada Twin Otter atmospheric research aircraft. A summary of the aircraft observations, instrument description, data processing and preliminary flux estimates for the run-averaged data for each flux transect are given in the data report (MacPherson, 1998). A single flight track, ~15 km in length, was flown over the ER study area multiple times during each mission with the aircraft flying essentially east–west (see Fig. 3) at approximately 35 m above local ground level (agl). During the mid-morning aircraft survey on DOY 183 used here (starting at 10:33 AM Central Standard Time, or CST), winds at 35 m agl were 2.7 m s^{-1} from the SW. From eddy covariance flux data collected over the entire ER transect, Mahrt et al. (2001) computed segmented flux values over 1-km intervals, which they then sub-sampled using a 250-m moving window and a scheme for the estimating time–space dependence of surface fluxes.
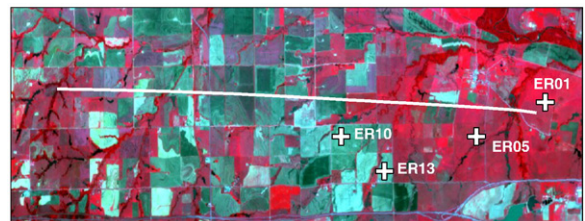

Fig. 3. RGB three-color composite image of the El Reno (ER) study area, generated with TMS bands 7–5–3 (NIR–Red–Green). Line indicates aircraft transect, and crosses show ER sampling and tower locations referenced in the text. (For interpretation of the references to color in this figure legend, the reader is referred to the web version of this article.)

3.3. Aircraft remote sensing data

High-resolution surface radiometric temperature, vegetation cover, and land-use maps were derived from images acquired with the Thermal Infrared Multispectral Scanner (TIMS) and the Thematic Mapper Simulator (TMS), flown by aircraft over the ER site. The TIMS instrument is a six-channel scanner operating in the thermal infrared (8–12 μm) region of the electromagnetic spectrum, while TMS simulated the Landsat TM bands and was used to create maps of NDVI. Both sensors were flown on a DOE Cessna Citation aircraft at ~5 km agl, yielding a ground resolution of approximately 12 m. To accurately rectify and co-register the TMS and TIMS imagery, TIMS and TMS data were re-sampled and then aggregated to 30 m. The average TIR sensor viewing angle used in the analysis was on the order of 10°. The El Reno flight lines provided coverage of an area approximately 8 km north–south by 28 km east–west. Further details concerning the processing of these data, including corrections for emissivity and atmospheric effects, are provided by French et al. (2000a,b). Additionally, a map of land-use/land-cover in the modeling domain was created by a supervised maximum-likelihood classification scheme using TMS imagery from DOY 183. The TIMS/TMS data on DOY 183 were collected at approximately 10:20 AM CST.

Soil moisture fields used in the soil respiration model were generated from microwave imagery collected at L-band by the ESTAR (Electronically Scanned Thinned Array Radiometer) instrument, flown periodically over ER during SGP97 on a P-3 aircraft operated by NASA's Wallops Flight Center. Details of the processing of the ESTAR data and the moisture retrieval algorithm are given by Jackson et al. (1999). The derived soil moisture product has a spatial resolution of 800 m and represents volumetric moisture content in the 0–5 cm layer. Given that the soil drying rate typically decreases with depth, this 0–5 cm estimate may somewhat underestimate the 0–10 cm value required by Eq. (4). Comparisons of microwave soil moisture estimates from SGP97 with ground-based measurements of volumetric soil moisture in the 0–5 cm layer yielded errors of approximately 3% (Jackson et al., 1999). The ESTAR data used in this study were collected at 10:25 CST on DOY 183.

3.4. Tower fluxes and ancillary measurements

Tower observations of energy and water fluxes were collected at several locations within the ER study area with eddy covariance instrumentation mounted at 2 m agl, recording half-hourly averaged fluxes. Twine et al. (2000) provide detailed description of the observations and an analysis of the measurement uncertainties. The data used here were collected over a 2 week period (DOY 180–195) at the ER01JPBK and ERO5JPBK towers (see Table 2 in Twine et al., 2000), situated in rangeland with average local LAI of 4.2 and 2.6 respectively (Fig. 3). Meteorological data, including air temperature, vapor pressure and windspeed, were measured at 2 m agl, and measurements of net radiation, insolation and the soil heat conduction flux were also collected. Canopy height and LAI were measured periodically at each tower site, the latter with a LICOR LAI-2000 Plant Canopy Analyzer[1] (Welles and Norman, 1991), with care taken to sample the local heterogeneity in vegetation cover conditions.

3.5. Soil respiration and ancillary measurements

Measurements of soil respiration and the input data required in Eq. (4) were made at 10 locations within each of several sites in the SGP97 study area. A LICOR LI-6000-09 soil chamber was used with a LI-6262 infrared gas analyzer operated in absolute mode by main-

Table 2
Quantitative measures of TSEB model performance[a] in estimating half-hourly daytime fluxes measured at individual EC towers in the ER study area

Flux	N	$\bar{O}$	MBE	RMSD	r^2	E	%
		$\overline{\text{W m}^{-2}}$	$\overline{\text{W m}^{-2}}$	$\overline{\text{W m}^{-2}}$			error
Bowen ratio closure							
PT							
RN	698	420	−3	29	0.98	0.98	5
LE	698	335	47	79	0.90	0.76	19
H	698	54	−53	69	0.68	0.09	107
G	698	31	3	28	0.32	0.31	69
All	2792	210	−1	56	0.95	0.94	19
LUE							
RN	698	420	−4	30	0.98	0.98	5
LE	698	335	24	48	0.93	0.91	11
H	698	54	−34	50	0.82	0.51	70
G	698	31	6	23	0.59	0.52	59
All	2792	210	−2	40	0.97	0.97	14
Residual closure							
PT							
RN	694	421	−3	29	0.98	0.98	5
LE	694	351	32	66	0.92	0.84	15
H	694	39	−38	51	0.72	0.32	110
G	694	31	3	28	0.32	0.31	69
All	2776	210	1	46	0.97	0.96	16
LUE							
RN	694	421	4	30	0.98	0.98	5
LE	694	351	9	40	0.94	0.94	9
H	694	39	−19	39	0.90	0.61	78
G	694	31	6	23	0.59	0.52	59
All	2776	210	−2	34	0.98	0.98	12

[a] Here N is the number of observations, $\bar{O}$ is the mean observed flux, RMSD is the root-mean-square difference between the modeled (P) and observed (O) quantities, MBE is the mean bias error ($\bar{P}-\bar{O}$), r^2 is the coefficient of determination in a linear regression of P on O, E is the coefficient of efficiency, and the percent error is defined as the mean absolute difference between P and O divided by the mean observed flux.

taining the reference cell at a zero concentration of CO_2. The respiration flux was calculated from the equations in the LI-6000-09 instruction manual using the drawdown in CO_2 concentration over a period of several minutes. The soil collars were installed about 2 cm into the soil 4–24 h prior to data collection. Soil temperature was measured at 2-cm and 10-cm depths with a digital thermometer having a 20-cm length steel probe, while soil volumetric moisture content for the 0–10 cm depth was calculated from gravimetric water content and bulk density measurements. Leaf area index was measured with a LAI-2000 at each of the 10 sampling locations at each site.

3.6. Energy budget closure corrections

By definition, the TSEB forces closure amongst the considered energy budget components (Eq. (3)). In contrast, the eddy covariance flux measurement technique does not enforce closure because the turbulent fluxes H and LE are measured independent of the available energy, RN–G. Closure, defined as the ratio (H+LE)/(RN–G), in tower EC fluxes from SGP97 ranged from 70–90% (Twine et al., 2000). EC closure errors may represent systematic undersampling of LE and/or H, an unsampled energy sink (e.g., energy consumed in photosynthesis; Meyers and Hollinger, 2004), unrepresentative sampling of RN–G (Anderson et al., 2004), or differences in source area on the land-surface contributing to each of these fluxes (Kustas et al., 2006).

Given these observational uncertainties, EC flux measurements are often adjusted to enforce closure when comparing with surface energy balance model results. In this way, we can better isolate potential instrumental components of model-measurement disagreement from actual modeling errors. Here, two common closure methods have been used: 1) augmenting both H and LE while retaining the observed Bowen ratio (BR) H/LE (Twine et al., 2000), and 2) assigning the entire residual to the latent heat flux (Li et al., 2005; Prueger et al., 2005).
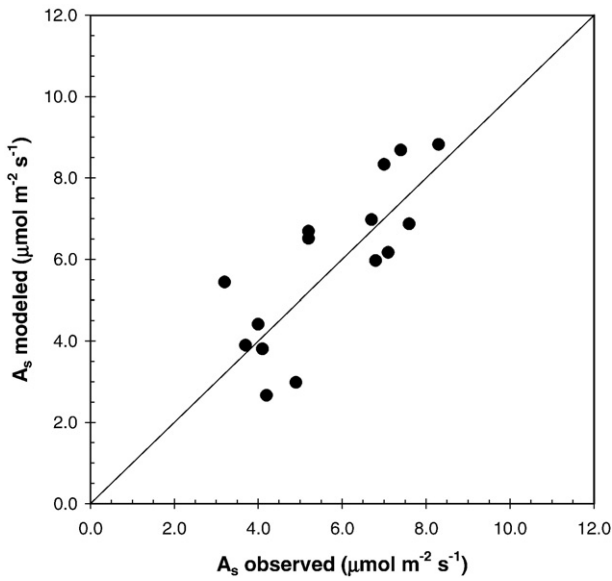
Fig. 4. Comparison between measurements made during SGP97 (rangeland) and predictions of soil respiration generated with an empirical function generated using FIFE data (tall-grass prairie).

4. Local application using in-situ data: comparison with ground-based flux observations

4.1. Soil respiration

To verify that the parameters derived for the soil respiration model based on FIFE data in tall-grass prairie are reasonably appropriate for carbon flux assessments over the ER landscape, Eq. (4) was tested using the in-situ measurements made during SGP97. Fig. 4 shows a comparison of modeled and measured A_S, yielding a mean absolute difference (MAD) of 1.0 μmol m^{-2} s^{-1} or 20% of the mean observed flux, a mean bias error (MBE) of 0.2 μmol m^{-2} s^{-1}, and a correlation coefficient of 0.8. The root-mean-square error is 1.2 μmol m^{-2} s^{-1}, identical to the error obtained in the original FIFE experiment (Norman et al., 1992). These results suggest that Eq. (4) should yield reasonable estimates of A_S over the ER domain during this time period, provided the remote sensing inputs are of good quality.

4.2. TSEB-tower comparisons

To assess the best-case performance of the modeling system over the ER landscape, the TSEB was run with both the PT and LUE transpiration subroutines (TSEB_PT and TSEB_LUE, respectively) at the ER01 and ER05 meteorological stations using in-situ measurements.
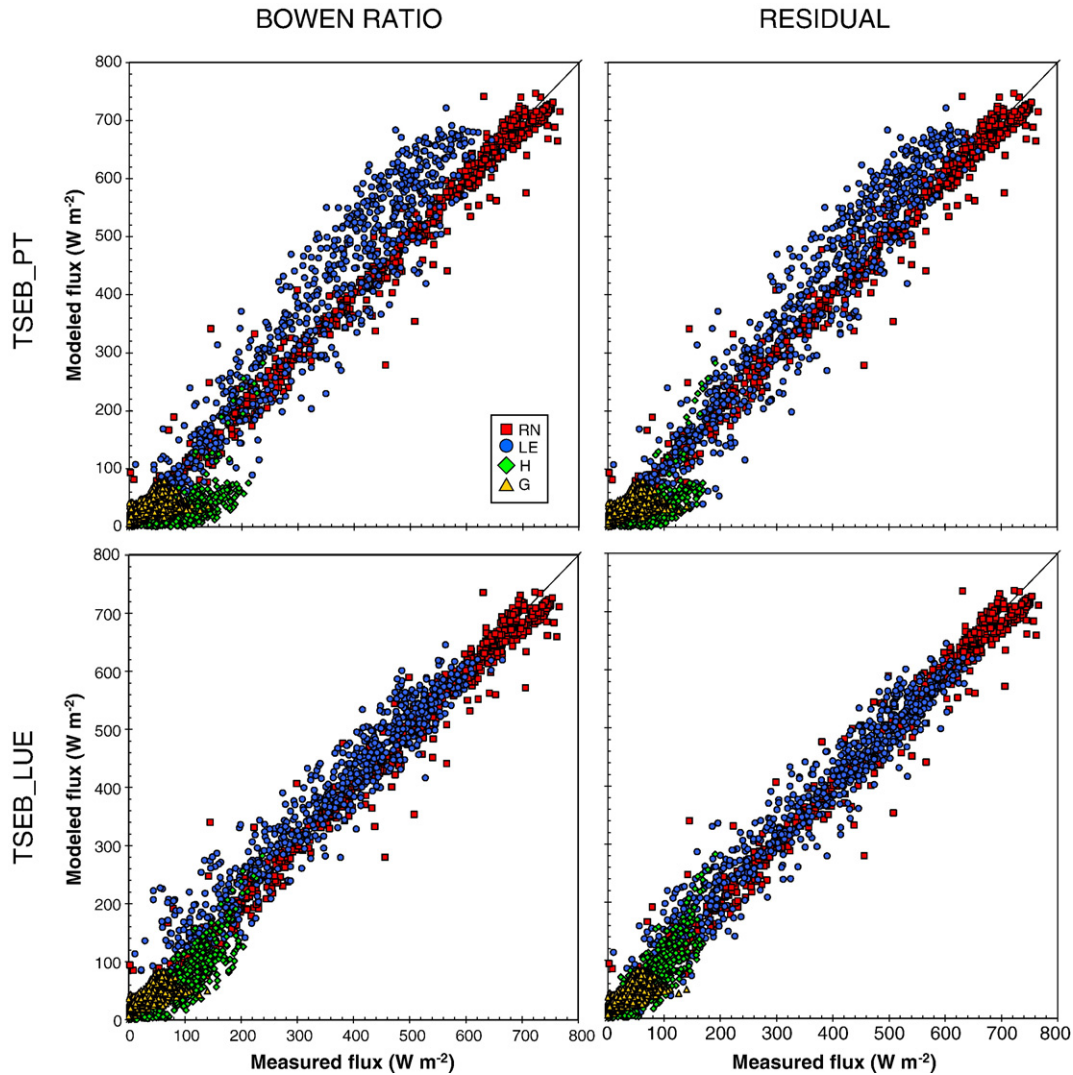

Fig. 5. Estimates of the major energy budget components generated with the TSEB_PT (top line) and TSEB_LUE (bottom line) models compared with tower flux measurements at ERO1 and ER05, adjusted using the BR (left column) and residual (right column) closure techniques.

Local observations of LAI and canopy height, and tower-based measurements of surface temperature, insolation, wind speed, air temperature and humidity were used as model inputs. Given the canopy composition at these sites, model LUE parameter values representing a mixture of C3 and C4 grasses from Anderson et al. (2000; see also Table A3) were used in TSEB_LUE. While carbon flux was not measured at these towers, the impact of the LUE vs. PT models on canopy transpiration and therefore overall energy budget partitioning can be assessed in comparison with tower observations of RN, G, H and LE.

Half-hourly predictions of energy budget components are compared with the tower measurements in Fig. 5, with related statistics in Table 2. Included in Table 2 is the coefficient of efficiency (E) proposed by Nash and Sutcliffe (1970) as a performance metric preferable to the coefficient of determination (r^2), which can indicate perfect agreement even in the presence of systematic model biases. As indicated in Table 2, both the PT and LUE modeling approaches yield better agreement with measurements closed using the residual method than the BR method. This is consistent with findings from other experiments comparing the TSEB with tower flux data (Li et al., 2006; Li et al., 2008), and may reflect a real difference in the way in which H and LE are transported by turbulent eddies and therefore sampled with an EC system (Prueger et al., 2005). It may also relate to the fact that LE_S is computed as a residual in the TSEB (Eq. (3)) — all components of the energy budget not explicitly accounted for in the TSEB (e.g., canopy heat and photosynthetic energy storage) are in effect accumulated in the modeled LE flux.

While both models reproduce observed fluxes with good accuracy, the TSEB_LUE formulation gives better overall agreement, particularly at site ER01 — the site with denser vegetation cover. Based on the residual-closed observations, the TSEB_LUE yields a root-mean-square deviation (RMSD) in LE of 40 W m^{-2} or 9% error (defined as in Table 1), compared to 66 W m^{-2} (15%) from the TSEB_PT. Similarly, RMSD in H is reduced from 51 to 39 W m^{-2}. For all energy balance components combined, TSEB_LUE and TSEB_PT produce RMSD values of 34 and 46 W m^{-2} (12% and 16%), respectively. The PT model has a greater tendency to partition too large a fraction of the available energy (RN–G) to latent heating, and this causes H to be underestimated. Apparently the LUE response to surface layer vapor pressure, land-surface temperature, and other driving factors is more effective than the PT coefficient modification algorithm in terms of reducing midday transpiration fluxes from the potential rate. TSEB_PT has no mechanism for reducing the PT coefficient unless LE_S goes below 0, which did not happen during this time period.

The effect of the choice of nominal LUE, β_n, on TSEB_LUE estimates of carbon assimilation and energy budget partitioning is demonstrated in Fig. 6. In using $\beta_n = 0.025$ (C3/C4 grass mix) instead of $\beta_n = 0.03$ (pure C4 stand), A_C is decreased to 72% of the C4 value, roughly in proportion to the ratio of nominal LUE values (0.8). The effect on energy budget partitioning, however, is minimal: LE is reduced by only 1% on average. These results suggest that while realistic values of β_n are critical for modeling carbon fluxes accurately, the exact value of β_n is not so important for determining the energy budget. Note that mechanistic photosynthesis models are also very sensitive to choice of primary model parameters, such as the maximum photosynthesis rate, V_{max} (e.g., Dang et al., 1998).

5. Regional application using remote sensing: comparison with aircraft fluxes

5.1. Soil respiration mapping

To map soil respiration using Eq. (4), estimates of θ_{10} were obtained from a soil moisture map derived from ESTAR microwave imagery obtained on DOY 183. Because the microwave soil moisture retrievals effectively sample only the top few cm of the soil profile, it is
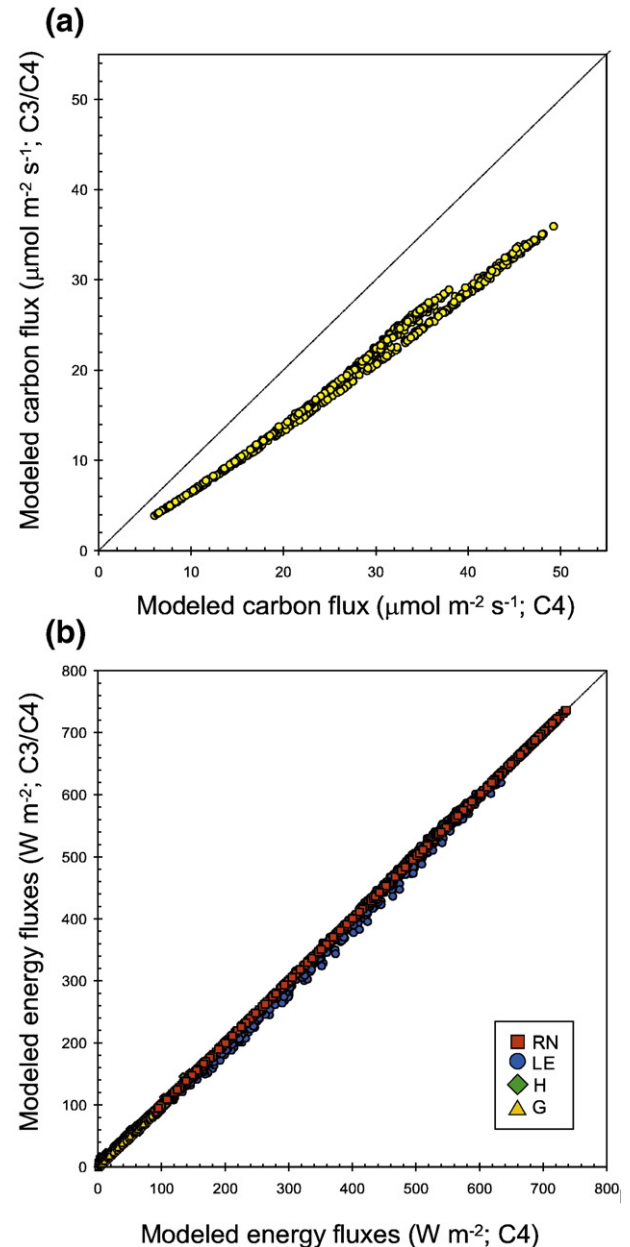

Fig. 6. Impact of choice of nominal LUE (β_n) parameter value on a) carbon flux estimates and b) energy budget partitioning, comparing results using β_n for a C3/C4 mixed canopy and β_n for a pure C4 grass stand.

likely that θ_{10} and therefore A_S are underestimated, particularly in areas of low vegetation cover where the soil surface skin can dry quickly after a rainfall. However, the magnitude of A_S in Eq. (4) is linear in LAI, so the overall flux in low cover areas should also be small.

Soil temperature at depth $z = 10$ cm ($T_{S,10}$) was computed by interpolating between the soil surface temperature (T_S) derived by the TSEB and a climatological deep soil temperature (T_d, held constant at 20 °C across the domain) using an exponential weighting function:

$$T(z) = T_d + (T_S - T_d) \exp\left(\frac{-z}{D}\right) \tag{5}$$

where D is the thermal damping depth, assumed to be 10 cm for the loam soils characteristic of the ER study area.

Fractional vegetation cover at nadir view, $f(0)$, was computed from the TMS NDVI data using the scaled relationship given by Choudhury et al. (1994), and LAI was then estimated using Eq. (2). The modeled

LAI agrees to within 0.3 with LAI-2000 measurements taken at ER01, ER05, and ER13, sampling a range in LAI from 0 to 4.

5.2. Flux maps

To investigate spatial patterns in surface fluxes over the ER study area, the regional form of the TSEB_LUE (DisALEXI_LUE) was executed with the TIMS/TMS imagery as described by Norman et al. (2003) and Kustas et al. (2006), but using the LUE submodel for LE_C in place of the PT submodel. As described in Section 2.1 and Table 1, DisALEXI_LUE uses air temperature boundary conditions diagnosed by the ALEXI model and vapor pressure data analyzed from standard synoptic observations in place of local tower observations, and therefore can be readily applied in areas where local data are not available. In this simulation, LUE parameters for C3/C4 grass mixture were used for classes representing rangeland and pasture (typically the redder regions in Fig. 3), while C3 parameters were used at pixels classified as wheat and alfalfa (Table A3).

Maps of component and system fluxes of CO_2 and latent heating are shown in Fig. 7, demonstrating the soil–canopy partitioning predicted by the two-source land-surface representation in DisALEXI_LUE. For comparison, the two primary remote sensing inputs to DisALEXI_LUE, NDVI and T_{RAD}, are also shown. The maps of canopy transpiration (LE_C) and assimilation (A_C) are well correlated with NDVI ($R^2 = 0.94$ for both) and with each other ($R^2 = 0.96$). In the absence of vegetation stress, these canopy fluxes should scale roughly in proportion to LAI.

Fig. 7 also shows a map of A_S modeled over the ER domain, with most values falling between 2 and 9 μmol m^{-2} s^{-1}, consistent with the range of the observed respiration measurements taken over the SGP97 study area. The modeled respiration fluxes are highest in the well-vegetated rangeland in the southeast quadrant of the domain, where ESTAR detected enhanced soil moisture conditions. This area had indeed obtained higher cumulative rainfall during SGP97 prior to DOY 183 (Jackson et al., 1999).

The modeled soil evaporation rate on DOY 183, four days after the last rainfall event (on DOY 179), is generally low across the domain (160 W m^{-2} on average). Based on the radiometric surface temperature data, however, DisALEXI_LUE identified a few wheat fields with low NDVI in the central part of the domain that had surface temperatures cool enough to require relatively high soil evaporation rates (250–350 W m^{-2}) to satisfy the surface energy balance. Fields A and B highlighted in Fig. 8, for example, have a green vegetation cover fraction similar to that in surrounding wheat fields (e.g., Field C in Fig. 8), but considerably lower surface temperature (37 vs. 45 °C) and are therefore diagnosed with higher soil evaporation (300 vs. 110 W m^{-2}). The enhanced evaporative flux in Fields A and B may be due to sheltering effects of standing (unharvested) senesced wheat. While Field C (an SGP97 sampling site: ER10) was known to be in harvested wheat stubble on DOY 193, Fields A and B appear to have been undergoing harvest at the time of imaging. The field borders are spectrally similar to the wheat stubble in Field C, while the interior areas interior resemble ARS fields with mature but unharvested wheat. Such a pattern would be expected during harvest, as field borders are typically harvested first to accommodate the combine turning radius before the interior is harvested crosswise. The standing senesced wheat inside Fields A and B would not be reflected in the NDVI or green vegetation cover fraction, $f(\theta)$, but would have the effect of reducing wind speed and net radiation at the soil surface and therefore decreasing the rate of soil evaporation (see
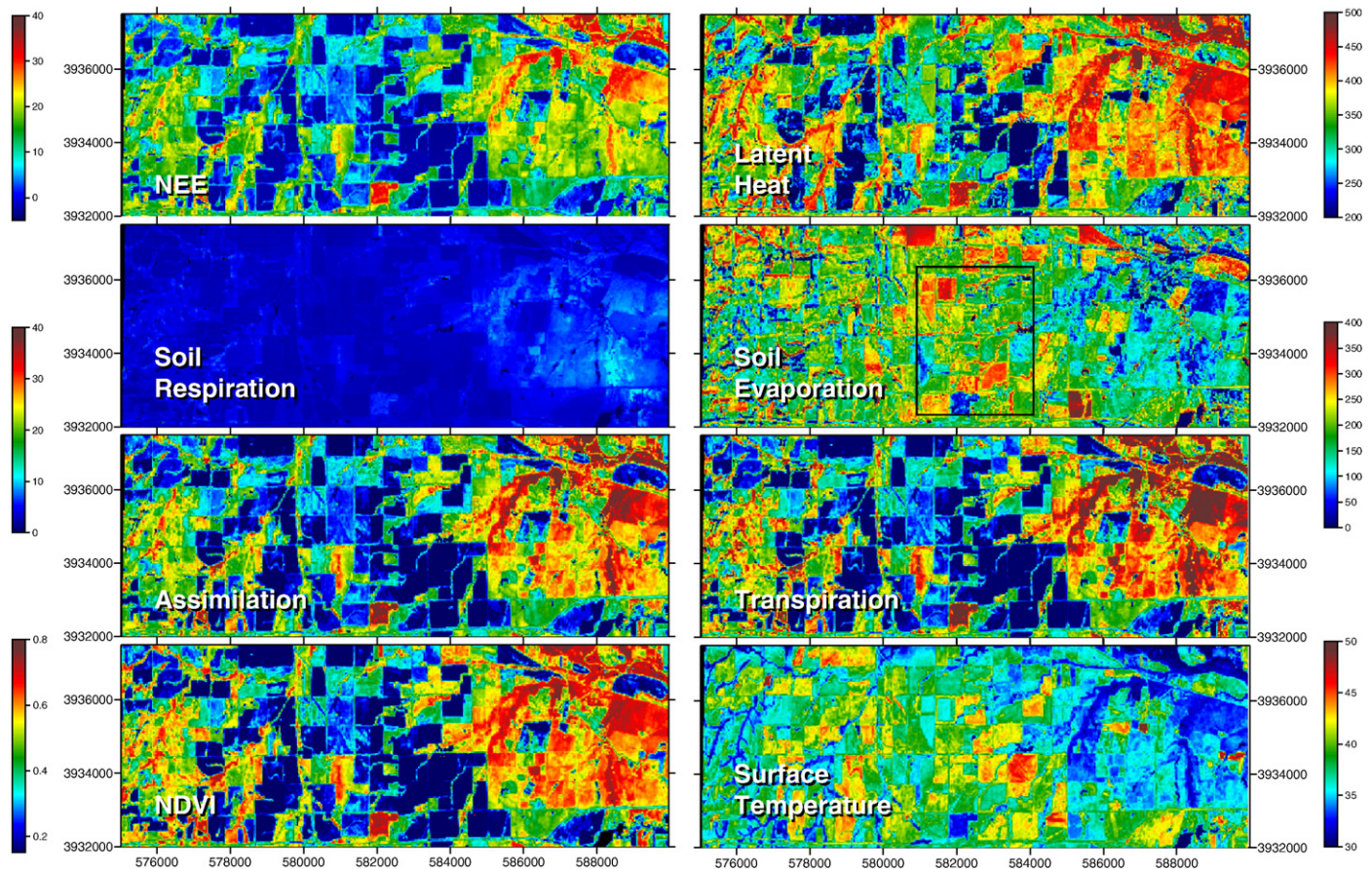

Fig. 7. Maps of soil, canopy, and system carbon (μmol m^{-2} s^{-1}) and latent heat flux (W m^{-2}) estimates from DisALEXI_LUE. Model input fields of NDVI and radiometric surface temperature, T_{RAD} (C), are also shown. Area demarcated in soil evaporation panel is expanded in Fig. 8.
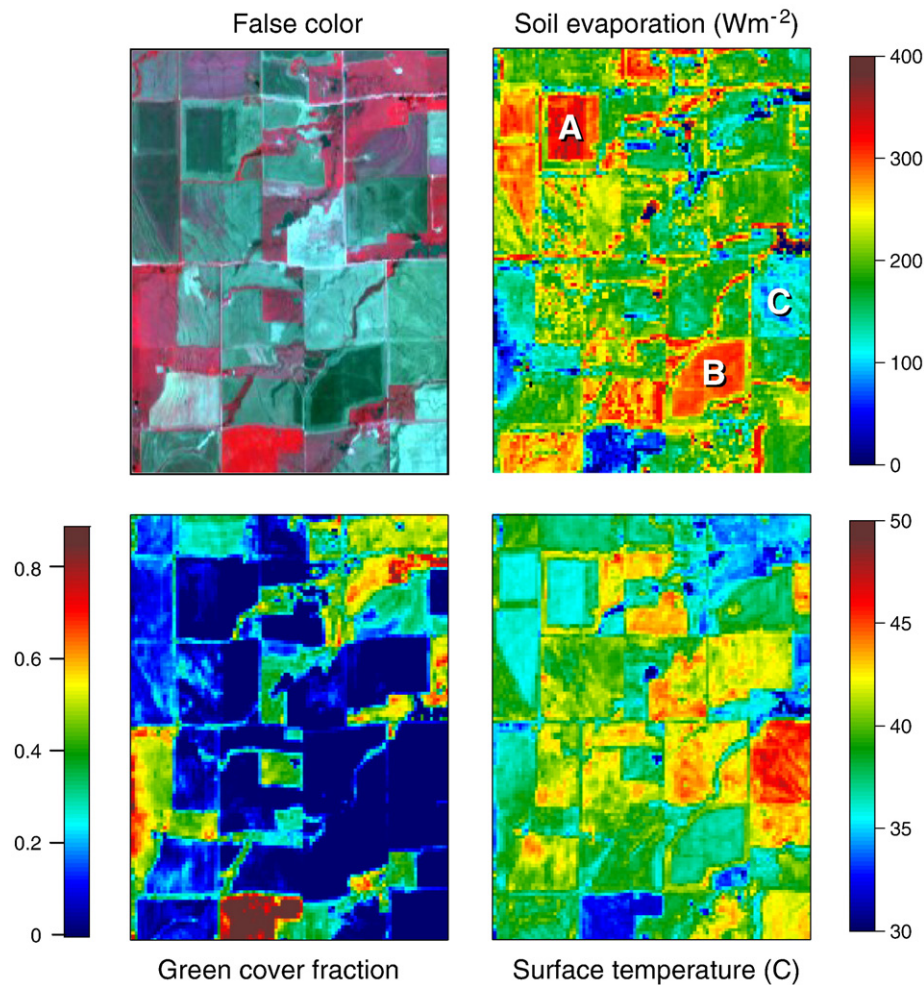
Fig. 8. Expanded view of region demarcated in Fig. 7, highlighting conditions in wheat fields diagnosed with low green vegetation cover and high soil evaporation rates (labeled A and B). In contrast, the modeled evaporation rates are much lower in an adjacent field (*C*) with similar cover fraction. The difference in moisture conditions between these fields may be related to residue cover amount.

also French et al., 2000a). This is an example of the value of the radiometric temperature inputs to the surface energy balance assessment: ET models based solely on indices sensitive to green vegetation cover (e.g., Szilagyi, 2002; Nagler et al., 2007) would detect little difference in ET between Fields A, B and C.

From Fig. 7, it is clear that the system (soil+canopy) fluxes are less well correlated with NDVI than are the canopy flux components. This is because soil evaporation and respiration are tied to moisture variability in the soil surface layer, which can vary strongly across the landscape due to patchy rainfall and drying. In this case, modeled LE in particular is not well predicted by NDVI alone (R^2=0.64) — the thermal data provide valuable additional information about the surface moisture status and direct soil evaporation.

5.3. DisALEXI-aircraft comparisons

Kustas et al. (2006) described the methods used to integrate the model surface fluxes along the ER transect for comparison with the airborne flux profiles. In short, the analytical flux footprint analysis technique of Schuepp et al. (1990, 1992), including a correction for atmospheric stability, was applied to DisALEXI_LUE output flux fields of *A* and LE. Footprint-weighted model fluxes were averaged over the 250 m interval/flux windows used to generate the aircraft flux profiles (Mahrt et al., 2001). Given the wind speed and stability conditions at the time of the overpass, the peak of the footprint function is offset ~250 m to the SW (upwind) of the transect.

Footprint-weighted net carbon and latent heat flux and LAI from DisALEXI_LUE are compared to the aircraft flux profiles in Fig. 9, showing good spatial agreement as the aircraft transits from vegetated pasture and riparian land in the west, over a broad region of low vegetation cover (harvested winter wheat) in the center part of the transect, and back to denser green vegetation cover in the east. Net flux magnitudes are well reproduced by the model (see statistical comparisons in Table 3). The agreement with the latent heat flux profile is similar to that obtained with DisALEXI_PT (Kustas et al., 2006).

In Fig. 9, the aircraft LE profiles are shown as measured and with a constant bias correction that enforces closure on average over the transect using both the residual and Bowen ratio methods, with the available energy (*RN*–*G*) in both cases coming from the footprint-weighted DisALEXI_LUE model output. Over most of the transect, the modeled LE is in better agreement with the BR-corrected aircraft fluxes (RMSD=35 W m^{-2}) than with the residual correction (RMSD=51 W m^{-2}), contrary to the findings with the 2-m tower fluxes discussed in Section 4.2. Given the measurement height, and the fact that *G* was not measured by the aircraft, the appropriate closure correction technique in this case is less clear. Kustas et al. (2006) and Anderson et al. (2007) note evidence for a difference in source area contributing to the *H* and LE fluxes measured by the aircraft, with sensible heat tending to correlate better with land-surface features in a swath directly under the aircraft flightpath, while latent heat was well reproduced by the footprint model, sampling the upwind fetch. Furthermore, some divergence in both *H* and LE is
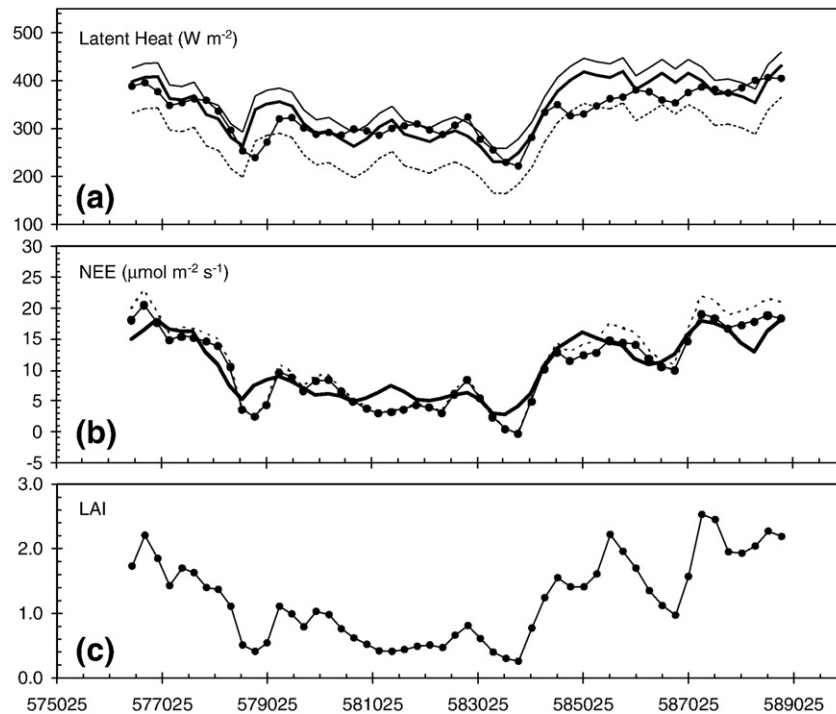
Fig. 9. Variation, from west to east, in segmented fluxes measured by aircraft over the ER transect and footprint-weighted output from the DisALEXI_LUE model assuming rangeland/ pastures with mixed C3/C4 composition (lines with circles): a) latent heat flux (W m^{-2}), with unclosed aircraft EC fluxes (dashed line), and fluxes closed with the BR (thick line) and residual (thin line) closure methods; b) Net Ecosystem Exchange (μmol m^{-2} s^{-1}), with unclosed aircraft EC fluxes (thick line), and model output assuming rangeland/pasture with pure C4 composition (dashed line); c) modeled LAI derived from NDVI imagery.

expected between 2 m and 35 m, and therefore the residual correction may be less appropriate at larger measurement heights. In general, LE from DisALEXI_LUE lies between the residual-corrected and unclosed fluxes, which may represent the bounds of uncertainty in the closure.

No closure correction was applied to the aircraft carbon flux measurements shown in Fig. 9. The observed profile shows good agreement (RMSD=2.3 μmol m^{-2} s^{-1}) with the mixed landscape simulation shown in Fig. 7, which assumes C3 parameter values for areas classified as wheat and alfalfa, and a C3/C4 mixture in the pasture and rangelands. In general, however, detailed information about grassland canopy composition may not be available. The dashed line in Fig. 8 demonstrates model sensitivity to the assumed composition, representing model results where the nominal LUE parameters for the rangeland/pasture class are assigned values associated with C4 grasses (Table A3). In this case, net carbon flux would be overestimated by 0.9 μmol m^{-2} s^{-1} (9% of the mean observed flux) on average along the transect (Table 3). Note that differences in LE generated under these two scenarios are very small, due in part to the relative insensitivity of LE to the value of β_n, and to the spatial averaging effected by the footprint model.

Table 3
Quantitative measures of DisALEXI_LUE model performance[a] in reproducing flux profiles measured over the aircraft transect

Flux	N	$\bar{O}$	MBE	RMSD	r^2	E	%
		$\overline{\text{W m}^{-2}}$	$\overline{\text{W m}^{-2}}$	$\overline{\text{W m}^{-2}}$			error
LE (residual[b]; C3/C4[c])	52	368	−40	51	0.68	0.18	11
LE (BR[d]; C3/C4)	52	340	−12	35	0.68	0.64	8
A (C3/C4)	52	10.5	−0.2	2.3	0.85	0.77	17
A (C4[e])	52	10.5	0.9	2.9	0.86	0.61	23

[a] Statistics are defined as in Table 1.
[b] Residual closure of observed energy budget.
[c] Mixed C3/C4 canopy composition assumed for pasture/rangeland.
[d] Bowen ratio (BR) closure of observed energy budget.
[e] Pure C4 canopy composition assumed for pasture/rangeland.

5.4. Light-use efficiency mapping

The dominant driver of variability in the effective LUE predicted by the DisALEXI_LUE model is land-cover class (C3 wheat vs. C3/C4 grass mixture). For both classes, however, the derived canopy LUE (β) has been decreased from the nominal class-specific values (β_n) in response to local atmospheric conditions and surface moisture deduced from the TIR inputs. LUE for pixels classified as rangeland was reduced from a nominal value of 0.025 mol mol^{-1} to an average of ~0.022 in most parts of the domain, while LUE for wheat classes was reduced from 0.020 to ~0.0165 mol mol^{-1} on average.

Fig. 10 maps the effective LUE (β) at 10:20 AM and the magnitude of the change from its nominal value ($\Delta\beta = \beta_n - \beta$) diagnosed by the analytical canopy resistance model in DisALEXI_LUE, focusing on the high-cover rangeland/pasture area in the eastern half of the domain (canopy light-use efficiency is ill-defined in areas of very low vegetation cover, so these areas have been blanked). Light-use efficiency is least modified in areas with lower surface radiometric temperature — primarily along riparian waterways where it can be assumed there is ample soil moisture supply. Using a coupled photosynthesis-canopy resistance model, Tuzet et al. (2003) demonstrated that in conditions of depleted rootzone moisture, where the soil matrix is unable to keep up with the noon-time atmospheric demand for water transpired by the canopy, a midday depression in the diurnal stomatal conductance and LUE curves will form and strengthen as the drying cycle progresses. In the ER landscape, midday depression effects should be less pronounced in the well-watered vegetation along the streambeds, as is predicted by the model.

6. Conclusions and future work

An analytical LUE-based model of bulk canopy resistance was effectively integrated into the diagnostic Two-Source Energy Balance (TSEB) model, enabling regional estimation of coupled carbon and water fluxes using thermal remote sensing data. Replacing the Priestley–Taylor
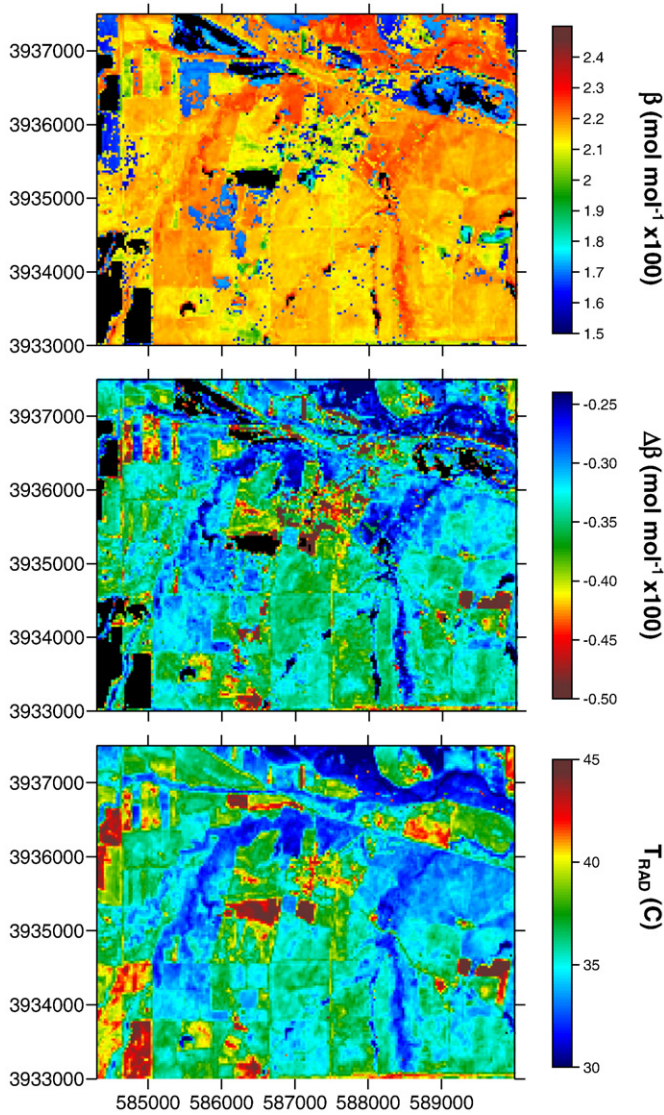
Fig. 10. Model estimates of effective light-use efficiency (β) and modification from the nominal class-dependent LUE value ($\Delta\beta$), and surface radiometric temperature mapped over rangeland and riparian areas in the eastern part of the ER domain.

vegetation indices will miss transient variability due to enhanced soil evaporation or vegetation stress.

The effective light-use efficiency, β, diagnosed by DisALEXI_LUE responds to local anomalies in the relationship between surface temperature and vegetation cover fraction. For a given cover fraction, cooler surface temperature is interpreted to indicate higher transpiration rate, and therefore higher canopy conductance and LUE. Future analyses will compare spatial variability in β predicted with the thermal-based DisALEXI_LUE with maps of LUE derived from short-wave indices, such as the Photochemical Reflectance Index (PRI; Drolet et al., 2008; Hall et al., 2008).

For comparison with airborne carbon flux observations, a simple empirical model of heterotrophic soil respiration based on LAI, soil moisture, and soil surface temperature (Eq. (4)) was used to convert modeled canopy assimilation fluxes to net ecosystem exchange. In mapping mode, soil moisture inputs were retrieved from L-band microwave data, LAI from NDVI, and soil temperature from the TSEB. However, passive microwave retrieval techniques are sensitive to soil moisture in only the upper few cm of the soil profile and may tend to underestimate the 0–10 cm moisture content (θ_{10}) used in Eq. (4). For future applications, the TSEB itself could be used to estimate θ_{10}, using functions based on the ratio of actual to potential evapotranspiration. Anderson et al. (2007a) and Hain et al. (2008) demonstrated that the TSEB reasonably reproduced spatial and temporal variability in soil moisture observations averaged down to 100 cm depth, with the component fluxes LE_S and LE_C adding some ability to distinguish between surface layer and root zone moisture.

For mapping applications with ALEXI at the continental scale, the challenge will be to obtain vapor pressure boundary conditions that are compatible with the surface radiometric temperature data — biases between these inputs have the potential to corrupt the partitioning of the energy budget. One possible approach is to use the saturation vapor pressure at the temperature of the land-surface as an indicator of the local vapor pressure deficit (Hashimoto et al., 2008). If a suitable vapor pressure data source can be identified, the ALEXI/DisALEXI system can facilitate nested mapping of carbon and water fluxes at local to continental scales, providing spatial context for interpreting and upscaling tower and aircraft flux and flask data collected over heterogeneous landscapes.

Acknowledgments

Appendix A

(PT) canopy transpiration module in the original TSEB (Norman et al., 1995) with an LUE-based module resulted in improved partitioning of the energy budget in comparison with tower observations collected during SGP97, with a reduction in prediction errors from 15 to 9% for the latent heat flux, and from 16 to 12% for all energy budget components combined. The PT approach tended to overestimate latent heat over well-vegetated rangeland sites, whereas the LUE module was able to achieve appropriate reductions in canopy conductance in response to elevated midday vapor pressure deficits.

When applied in mapping mode within the framework of the DisALEXI model, the analytical canopy resistance submodel generated spatial patterns in instantaneous surface carbon and latent heat fluxes that agree well with airborne measurements along a flight transect sampling rangeland, riparian areas, and harvested winter wheat fields. Spatial variability in the canopy component assimilation and transpiration fluxes correlate well with cover fraction and NDVI. Correlations between NDVI and system fluxes of ET and NEE, however, are degraded due to the soil flux components, which are tied strongly to soil moisture variations. This demonstrates the value added by the thermal remote sensing data, which carry information about the surface moisture status. ET mapping methods based purely on

Table A1
Equations of the TSEB_PT and TSEB_LUE models

Equation	Description	No.
TSEB_PT model		
$T_{RAD}(\theta) = [f(\theta)T_C^4 + [1-f(\theta)]T_S^4]^{1/4}$	Two-source partitioning of T_{RAD} at view angle θ	(A1)
$RN = H + LE + G$	System energy budget	(A2)
$RN_S = H_S + LE_S + G$	Soil component energy budget	(A3)
$RN_C = H_C + LE_C$	Canopy component energy budget	(A4)
$RN = RN_S + RN_C$	System net radiation	(A5)
$H = H_S + H_C = \rho c_p \dfrac{T_{AC} - T_A}{R_A}$	System sensible heat	(A6)
$H_S = \rho c_p \dfrac{T_S - T_{AC}}{R_S}$	Soil sensible heat	(A7)
$H_C = \rho c_p \dfrac{T_C - T_{AC}}{R_X}$	Canopy sensible heat	(A8)

Table A1 (continued)

Equation	Description	No.
TSEB_PT model		
$LE = LE_S + LE_C$	System latent heat	(A9)
$LE_C = \alpha_C f_g \dfrac{\Delta}{\Delta + \gamma_p} RN_C$	Initial estimate of canopy transpiration (TSEB_PT)	(A10)
$G = \alpha_g RN_S$	Soil conduction heat	(A11)
Analytical canopy resistance model in TSEB_LUE		
$LE_C = \lambda \dfrac{e*(T_C) - e_{AC}}{P(R_C + R_B)}$	Canopy transpiration (TSEB_LUE)	(A12)
$LE_C = \lambda \dfrac{e*(T_C) - e_B}{PR_C} = \lambda \dfrac{e*(T_C)[1 - RH_B]}{PR_C}$	Canopy transpiration (TSEB_LUE)	(A13)
$A_C = \dfrac{C_A - C_i}{(1.6 R_C + 1.3 R_B + R_{A,\mu m})}$	Canopy assimilation	(A14)
$A_C = \dfrac{C_A - C_B}{(1.3 R_B + R_{A,\mu m})}$	Canopy assimilation	(A15)
$R_b = (f_s / [f_g \times f_{dry}]) R_{x,\mu m}$	Bulk leaf boundary layer resistance governing transpiration and assimilation	(A16)
$\dfrac{1}{R_C} = b_C + m \dfrac{A_C RH_B}{C_B}$	Ball et al. (1986) equation for stomatal resistance, scaled to canopy level	(A17)
$b_C = b \times F \times f_{dry} \times f_g$	Upscaling of Ball et al. b parameter to canopy level	(A18)
$A_C = \beta(\gamma) APAR$	Canopy assimilation − LUE relationship	(A19)
$\gamma = C_i / C_A$	Intercellular-ambient CO_2 ratio (variable)	(A20)
$\beta(\gamma) = \dfrac{\beta_n}{(\gamma_n - \gamma_0)} (\gamma - \gamma_0)$	Linear function modifying the nominal LUE (β_n) in response to modeled C_i/C_A	(A21)

Table A2
Model variables and parameters

Symbol	Units	Description
TSEB_PT model		
α	–	Reflectivity of soil-canopy system
α_C	–	Priestley–Taylor coefficient for canopy transpiration (initial value of 1.3)
α_g	–	Soil heat flux coefficient (0.3)
Δ	kPa K^{-1}	Slope of saturation vapor pressure vs. temperature curve
F	–	Leaf area index
$f(\theta)$	–	Fractional vegetation cover at view angle θ
f_g	–	Fraction of green vegetation
G	W m^{-2}	Soil heat flux
γ_p	kPa K^{-1}	Psychrometer constant
H	W m^{-2}	System sensible heat flux
H_C	W m^{-2}	Canopy sensible heat flux
H_S	W m^{-2}	Soil sensible heat flux
λ	J kg^{-1}	Latent heat of vaporization
λE	W m^{-2}	System latent heat flux
λE_C	W m^{-2}	Canopy transpiration
λE_S	W m^{-2}	Soil evaporation
θ	deg	TIR sensor view angle from nadir
R_A	s m^{-1}	Aerodynamic resistance for momentum
R_x	s m^{-1}	Bulk two-sided leaf boundary layer resistance
R_S	s m^{-1}	Soil boundary layer resistance
RN	W m^{-2}	Net radiation above canopy[a]
RN_C	W m^{-2}	Net radiation divergence within canopy[a]
RN_S	W m^{-2}	Net radiation above soil surface[a]
ρc_p	J K^{-1} m^{-3}	Volumetric heat capacity of air
T_{AC}	K	Aerodynamic temperature
T_C	K	Canopy temperature
T_S	K	Soil surface temperature
$T_{RAD}(\theta)$	K	Surface radiometric temperature at view angle θ
Analytical canopy resistance model		
A_C	μmol m^{-2} s^{-1}	Canopy assimilation rate (positive downward)
$APAR$	μmol m^{-2} s^{-1}	Absorbed photosynthetically active radiation
b	μmol m^{-2} s^{-1}	Ball et al. (1986) offset parameter (leaf scale)
b_C	μmol m^{-2} s^{-1}	b scaled to canopy level
β_n	mol CO_2 mol^{-1} APAR	Nominal unstressed canopy LUE (model input)
β	mol CO_2 mol^{-1} APAR	Effective canopy LUE, including stress response (model output)
C_A	mol CO_2 mol^{-1} air	Ambient CO_2 concentration
C_B	mol CO_2 mol^{-1} air	CO_2 concentration in the leaf boundary layer
C_i	mol CO_2 mol^{-1} air	Substomatal CO_2 concentration
$e*(T_C)$	kPa	Saturation vapor pressure at canopy temperature
e_A	kPa	Ambient vapor pressure
e_{AC}	kPa	In-canopy vapor pressure

Table A2 (continued)

Symbol	Units	Description
Analytical canopy resistance model		
f_{dry}	–	Dry vegetation fraction
f_s	–	Stomatal distribution correction factor
γ	–	Ratio of intercellular to ambient CO_2 concentrations (C_i/C_A)
γ_n	–	Nominal value of γ
γ_0	–	Value of C_i/C_A at $\beta = 0$
λ	J μmol^{-1}	Latent heat of vaporization
m	–	Ball et al. (1986) slope parameter
P	kPa	Atmospheric pressure
$R_{A,\mu m}$	m^2 s μmol^{-1}	Aerodynamic resistance for momentum
R_B	m^2 s μmol^{-1}	Bulk leaf boundary resistance, corrected for stomatal distribution and dry green leaf area
R_C	m^2 s μmol^{-1}	Bulk canopy resistance
$R_{x,\mu m}$	m^2 s μmol^{-1}	Bulk two-sided leaf boundary layer resistance
RH_B	–	Relative humidity inside the leaf boundary layer
Soil respiration model and Net Ecosystem Exchange (NEE)		
A	μmol m^{-2} s^{-1}	Net Ecosystem Exchange ($A = A_C - A_S$; positive downward)
A_S	μmol m^{-2} s^{-1}	Soil respiration rate (positive upward)
D	m	Thermal damping depth
T_d	K	Climatological deep soil temperature
$T(z)$	K	Temperature at depth z (m)

[a] See App. B in Anderson et al. (2000) for equations for RN, RN$_S$ and RN$_C$.

Table A3
Canopy resistance model parameter values

Quantity	Symbol	Units	C4 grass	C3 grass	C3/C4
Nominal LUE	β_n	mol mol^{-1}	0.03	0.02	0.025
Nominal C_i/C_A ratio	γ_n	mol mol^{-1}	0.6	0.8	0.7
C_i/C_A at $\beta = 0$	γ_0	mol mol^{-1}	0.0	0.2	0.1
Ball & Berry slope	m		4.0	9.0	6.5
Ball & Berry offset	b	μmol m^{-2} s^{-1}	0.04×10^6	0.01×10^6	0.025×10^6

References

Anderson, M. C., Kustas, W. P., & Norman, J. M. (2003). Upscaling and downscaling — A regional view of the soil–plant–atmosphere continuum. *Agronomy Journal, 95*, 1408–1423.

Anderson, M. C., Kustas, W. P., & Norman, J. M. (2007). Upscaling flux observations from local to continental scales using thermal remote sensing. *Agronomy Journal, 99*, 240–254.

Anderson, M. C., Norman, J. M., Diak, G. R., Kustas, W. P., & Mecikalski, J. R. (1997). A two-source time-integrated model for estimating surface fluxes using thermal infrared remote sensing. *Remote Sensing of Environment, 60*, 195–216.

Anderson, M. C., Norman, J. M., Mecikalski, J. R., Otkin, J. P., & Kustas, W. P. (2007). A climatological study of evapotranspiration and moisture stress across the continental U.S. based on thermal remote sensing: I. Model formulation. *Journal of Geophysical Research, 112*(D10117). doi:10.1029/2006JD007506

Anderson, M. C., Norman, J. M., Mecikalski, J. R., Otkin, J. P., & Kustas, W. P. (2007). A climatological study of evapotranspiration and moisture stress across the continental U.S. based on thermal remote sensing: II. Surface moisture climatology. *Journal of Geophysical Research, 112*(D11112). doi:10.1029/2006JD007507

Anderson, M. C., Norman, J. M., Mecikalski, J. R., Torn, R. D., Kustas, W. P., & Basara, J. B. (2004). A multi-scale remote sensing model for disaggregating regional fluxes to micrometeorological scales. *Journal of Hydrometeorology, 5*, 343–363.

Anderson, M. C., Norman, J. M., Meyers, T. P., & Diak, G. R. (2000). An analytical model for estimating canopy transpiration and carbon assimilation fluxes based on canopy light-use efficiency. *Agricultural and Forest Meteorology, 101*, 265–289.

Arkebauer, T. J., Weiss, A., Sinclair, T. R., & Blum, A. (1994). In defense of radiation use efficiency: a response to Demetriades-Shah. *Agricultural and Forest Meteorology, 68*, 221–227.

Avissar, R. (1993). Observations of leaf stomatal conductance at the canopy scale: an atmospheric modeling perspective. *Boundary - Layer Meteorology, 64*, 127–148.

Baldocchi, D. D., & Wilson, K. B. (2001). Modeling CO_2 and water vapor exchange of a temperate broadleaved forest across hourly to decadal time scales. *Ecological Modelling, 142*, 155–184.

Ball, J. T., Woodrow, I. E., & Berry, J. A. (1986). A model predicting stomatal conductance and its contribution to the control of photosynthesis under different environmental conditions. In J. Biggins (Ed.), *Progress in photosynthesis research* (pp. 221–225). Dodrecht: Nijhoff.

Berry, J.A., and Farquhar, G.D. (1978), The CO2 concentrating function of C4 photosynthesis: A biochemical model, paper presented at 4th International Congress on Photosynthesis, Biochemical Society, London.

Betts, A. K., Chen, F., Mitchell, K. E., & Janjic, Z. I. (1997). Assessment of the land surface and boundary layer models in two operational versions of the NCEP Eta model using FIFE data. *Monthly Weather Review, 125*, 2896–2916.

Choudhury, B. J., Ahmed, N. U., Idso, S. B., Reginato, R. J., & Daughtry, C. S. T. (1994). Relations between evaporation coefficients and vegetation indices studied by model simulations. *Remote Sensing of Environment, 50*, 1–17.

Collatz, G. J., Ribas-Carbo, J., & Berry, J. A. (1992). Coupled photosynthesis-stomatal conductance model for leaves of C4 plants. *Australian Journal of Plant Physiology, 19*, 519–538.

Coudert, B., & Ottlé, C. (2007). An improved SVAT model calibration strategy based on the optimisation of surface temperature temporal dynamics. *Geophysical Research Letters, 34*(L04402). doi:10.1029/2006GL028778

Coudert, B., Ottlé, C., & Briottet, X. (2008). Monitoring land surface processes with thermal infrared data: Calibration of SVAT parameters based on the optimisation of diurnal surface temperature cycling features. *Remote Sensing of Environment, 112*, 872–887.

Dang, Q. L., Margolis, H. A., & Collatz, G. J. (1998). Parameterization and testing of a coupled photosynthesis-stomatal conductance model for boreal trees. *Tree Physiology, 18*, 141–153.

Diak, G. R., Mecikalski, J. R., Anderson, M. C., Norman, J. M., Kustas, W. P., Torn, R. D., et al. (2003). Estimating land-surface energy budgets from space: Review and current efforts at the University of Wisconsin-Madison and USDA-ARS. *Bulletin of the American Meteorological Society, 85*, 65–78.

Drolet, G. G., Middleton, E. M., Huemmrich, K. F., Hall, F. G., Amiro, B. D., Barr, A. G., et al. (2008). Regional mapping of gross light-use efficiency using MODIS spectral indices. *Remote Sensing of Environment, 112*, 3064–3078.

Farquhar, G. D., von Caemmerer, S., & Berry, J. A. (1980). A biochemical model of photosynthetic CO_2 assimilation in leaves of C3 plants. *Plant, 149*, 78–90.

French, A. N., Schmugge, T. J., & Kustas, W. P. (2000). Discrimination of senescent vegetation using thermal emissivity contrast. *Remote Sensing of Environment, 74*, 249–254.

French, A. N., Schmugge, T. J., & Kustas, W. P. (2000). Surface fluxes over the SGP site with remotely sensed data. *Physics and Chemistry of the Earth (B), 25*, 167–172.

French, A. N., Schmugge, T. J., Kustas, W. P., Brubaker, K. L., & Prueger, J. (2003). Surface energy fluxes over El Reno, Oklahoma, using high-resolution remotely sensed data. *Water Resources Research, 39*. doi:10.1029/2002WR001734

Gillies, R. R., & Carlson, T. N. (1995). Thermal remote-sensing of surface soil–water content with partial vegetation cover for incorporation into climate models. *Journal of Applied Meteorology, 34*, 745–756.

Goetz, S. J., & Prince, S. D. (1998). Modeling terrestrial carbon exchange and storage: The evidence for and implications of functional convergence in light use efficiency. In A. H. Fitter & D. Raffaelli (Eds.), *Advances in ecological research* (pp. 57–92). San Diego: Academic Press.

Gollan, T., Passioura, J. B., & Munns, R. (1986). Soil water status affects the stomatal conductance of fully turgid wheat and sunflower leaves. *Australian Journal of Plant Physiology, 13*, 459–464.

Gower, S. T., Kucharik, C. J., & Norman, J. M. (1999). Direct and indirect estimation of leaf area index, fAPAR and net primary production of terrestrial ecosystems. *Remote Sensing of Environment, 70*, 29–51.

Hain, C. R., Mecikalski, J. R., & Anderson, M. C. (2008). A thermal infrared-based (TIR) retrieval of soil moisture. Part I: Methodology and validation. *Journal of Hydrology*.

Hall, F. G., Hilker, T., Coops, N. C., Lyapustin, A., Huemmrich, K. F., Middleton, E. M., et al. (2008). Multi-angle remote sensing of forest light use efficiency by observing PRI variation with canopy shadow fraction. *Remote Sensing of Environment, 112*, 3201–3211.

Hashimoto, H., Dungan, J. L., White, M. A., Yang, F., Michaelis, A. R., Running, S. W., et al. (2008). Satellite-based estimation of surface vapor pressure deficits using MODIS land surface temperature data. *Remote Sensing of Environment, 112*, 142–155.

Jackson, T. J., Le Vine, D. M., Hsu, A. Y., Oldak, A., Starks, P. J., Swift, C. T., et al. (1999). Soil moisture mapping at regional scales using microwave radiometry: The Southern Great Plains hydrology experiment. *IEEE Transactions on Geoscience and Remote Sensing, 37*, 2136–2151.

Jarvis, P. G. (1976). The interpretation of the variations in leaf water potential and stomatal conductance found in canopies in the field. *Philosophical Transactions of the Royal Society of London Series B, 273*, 593–610.

Kim, S. H., & Lieth, J. H. (2003). A coupled model of photosynthesis, stomatal conductance, and transpiration for a rose leaf (*Rosa hybrida* L.). *Annals of Botany, 91*, 771–781.

Kustas, W. P., Li, F., Jackson, T. J., Prueger, J. H., MacPherson, J. I., & Wolde, M. (2004). Effects of remote sensing pixel resolution on modeled energy flux variability of croplands in Iowa. *Remote Sensing of Environment, 94*, 535–547.

Kustas, W. P., & Norman, J. M. (1999). Evaluation of soil and vegetation heat flux predictions using a simple two-source model with radiometric temperatures for partial canopy cover. *Agricultural and Forest Meteorology, 94*, 13–25.

Kustas, W. P., & Norman, J. M. (1999). Reply to comments about the basic equations of dual-source vegetation-atmosphere transfer models. *Agricultural and Forest Meteorology, 94*, 275–278.

Kustas, W. P., & Norman, J. M. (2000). A two-source energy balance approach using directional radiometric temperature observations for sparse canopy covered surfaces. *Agronomy Journal, 92*, 847–854.

Kustas, W. P., Anderson, M. C., French, A. N., & Vickers, D. (2006). Using a remote sensing field experiment to investigate flux footprint relations and flux sampling distributions for tower and aircraft-based observations. *Advances in Water Resources, 29*, 355–368.

Landsberg, J. J., Prince, S. D., Jarvis, P. G., McMurtrie, R. E., Luxmore, R., & Medlyn, B. E. (1997). Energy conversion and use in forests: the analysis of forest production in terms of radiation utilisation efficiency (e). In H. L. Gholtz (Ed.), *Use of remote sensing in the modeling of forest productivity* (pp. 273–298). New York: Kluwer Academic Publishers.

Leuning, R. (1990). Modeling stomatal behavior and photosynthesis of Eucalyptus grandis. *Australian Journal of Plant Physiology, 17*, 159–175.

Leuning, R. (1995). A critical appraisal of a combined stomatal-photosynthesis model for C3 plants. *Plant, Cell and Environment, 18*, 339–355.

Leuning, R., Kelliher, F. M., De Pury, D. G. G., & Schulze, E. D. (1995). Leaf nitrogen, photosynthesis, conductance and transpiration: scaling from leaves to canopies. *Plant, Cell and Environment, 18*, 1183–1200.

Li, F., Kustas, W. P., Prueger, J. H., Neale, C. M. U., & Jackson, T. J. (2005). Utility of remote sensing based two-source energy balance model under low and high vegetation cover conditions. *Journal of Hydrometeorology, 6*, 878–891.

Li, F., Kustas, W. P., Anderson, M. C., Prueger, J. H., & Scott, R. L. (2008). Effect of remote sensing spatial resolution on interpreting tower-based flux observations. *Remote Sensing of Environment, 112*, 337–349.

Li, F., Kustas, W. P., Anderson, M. C., Jackson, T. J., Bindlish, R., & Prueger, J. (2006). Comparing the utility of microwave and thermal remote-sensing constraints in two-source energy balance modeling over an agricultural landscape. *Remote Sensing of Environment, 101*, 315–328.

MacPherson, J. I. (1998). *NRC Twin Otter operations in the 1997 Southern Great Plains Experiment.* Ottawa, Canada: National Research Council of Canada 122 pp.

Mahrt, L., Vickers, D., & Sun, J. (2001). Spatial variations of surface moisture flux from aircraft data. *Advances in Water Resources, 24*, 1133–1142.

McAneney, K. J., & Itier, B. (1996). Operational limits to the Priestley–Taylor formula. *Irrigation Science, 17*, 37–43.

McNaughton, K. G., & Jarvis, P. G. (1991). Effects of spatial scale on stomatal control of transpiration. *Agricultural and Forest Meteorology, 54*, 269–301.

McNaughton, K. G., & Spriggs, T. W. (1986). A mixed-layer model for regional evaporation. *Boundary - Layer Meteorology, 74*, 262–288.

Meyers, T. P., & Hollinger, S. E. (2004). An assessment of storage terms in the surface energy balance of maize and soybean. *Agricultural and Forest Meteorology, 125*, 105–115.

Monteith, J. L. (1966). The photosynthesis and transpiration of crops. *Experimental agriculture, 2*, 1–14.

Monteith, J. L. (1977). Climate and the efficiency of crop production in Britain. *Philosophical transactions-Royal Society of London Series B, 281*, 277–294.

Moran, M. S. (2003). Thermal infrared measurement as an indicator of plant ecosystem health. In D. A. Quattrochi & J. Luvall (Eds.), *Thermal remote sensing in land surface processes* (pp. 257–282). Taylor and Francis.

Myneni, R. B., Maggion, S., Iaquinta, J., Privette, J. L., Gobron, N., Pinty, B., et al. (1995). Optical remote sensing of vegetation: modeling, caveats, and algorithms. *Remote Sensing of Environment, 51*, 169–188.

Nagler, P. L., Glenn, E. P., Kim, J., Emmerich, W., Scott, R. L., Huxman, T. E., et al. (2007). Relationship between evapotranspiration and precipitation pulses in a semiarid rangeland estimated by moisture flux towers and MODIS vegetation indices. *Journal of Arid Environments, 70*, 443–462.

Nash, L. E., & Sutcliffe, J. V. (1970). River flow forecasting through conceptual models — Part 1: A discussion of principles. *Journal of Hydrobiology, 10*, 282–290.

Norman, J. M. (1979). Modeling the complete crop canopy. In B. J. Barfield, & J. F. Gerber (Eds.), *Modification of the aerial environment of plants* (pp. 249–277). St. Joseph, MI: Amer. Soc. Agric. Eng.

Norman, J. M., Anderson, M. C., Kustas, W. P., French, A. N., Mecikalski, J. R., Torn, R. D., et al. (2003). Remote sensing of surface energy fluxes at 101-m pixel resolutions. *Water Resources Research, 39*. doi:10.1029/2002WR001775

Norman, J. M., Garcia, R., & Verma, S. B. (1992). Soil surface CO_2 fluxes and the carbon budget of a grassland. *Journal of Geophysical Research, 97*, 18,845–818,853.

Norman, J. M., Kustas, W. P., & Humes, K. S. (1995). A two-source approach for estimating soil and vegetation energy fluxes from observations of directional radiometric surface temperature. *Agricultural and Forest Meteorology, 77*, 263–293.

Olioso, A., Chauki, H., Couralt, D., & Wigneron, J. P. (1999). Estimation of evapotranspiration and photosynthesis by assimilation of remote sensing data into SVAT models. *Remote Sensing of Environment, 68*, 341–356.

Potter, C., Klooster, S., Myneni, R. B., Genovese, V., Tan, P. N., & Kumar, V. (2003). Continental-scale comparisons of terrestrial carbon sinks estimated from satellite data and ecosystem modeling 1982–1998. *Global and Planetary Change, 39*, 201–213.

Priestley, C. H. B., & Taylor, R. J. (1972). On the assessment of surface heat flux and evaporation using large-scale parameters. *Monthly Weather Review, 100*, 81–92.

Prueger, J. H., Hatfield, J. L., Kustas, W. P., Hipps, L. E., MacPherson, J. I., & Parkin, T. B. (2005). Tower and aircraft eddy covariance measurements of water vapor, energy and carbon dioxide fluxes during SMACEX. *Journal of Hydrometeorology, 6*, 954–960.

Running, S. W., & Hunt, E. R. J. (1993). Generalization of a forest ecosystem process model for other biomes, BIOME-BGC, and an application for global-scale models. In J. R. Ehleringer & C.B. Field (Eds.), *Scaling physiological processes: Leaf to globe* (pp. 141–158). New York: Academic Press, Inc.

Schaake, J. C., et al. (2004). An intercomparison of soil moisture fields in the North American Land Data Assimilation System (NLDAS). *Journal of Geophysical Research, 109*. doi:10.1029/2002JD00309

Schuepp, P. H., Leclerc, M. Y., MacPherson, J. I., & Desjardins, R. L. (1990). Footprint prediction of scalar fluxes from analytical solutions of the diffusion equation. *Boundary - Layer Meteorology, 50*, 355–373.

Schuepp, P. H., MacPherson, J. I., & Desjardins, R. L. (1992). Adjustment of footprint correction for airborne flux mapping over the FIFE site. *Journal of Geophysical Research, 97*, 18,455–418,466.

Sellers, P. J., Hall, F. G., Asrar, G., Strebel, D. E., & Murphy, R. E. (1992). An overview of the first international satellite land surface climatology project (ISLSCP) field experiment (FIFE). *Journal of Geophysical Research, 97*, 18,345–318,371.

Sellers, P. J., Randall, D. A., Collatz, G. J., Berry, J. A., Field, C. B., Dazlich, D. A., et al. (1996). A revised land surface parameterization (SiB2) for atmospheric GCMs. Part I: Model formulation. *Journal of Climate, 9*, 676–705.

Smith, R. C. G., Barrs, H. D., Steiner, J. L., & Stapper, M. (1985). Relationship between wheat yield and foliage temperature: Theory and its application to infrared measurements. *Agricultural and Forest Meteorology, 36*, 129−143.

Stannard, D. I. (1993). Comparison of Penman–Monteith, Shuttleworth–Wallace, and modified Priestley–Taylor evapotranspiration models for wildland vegetation in semiarid rangeland. *Water Resources Research, 29*, 1379−1392.

Szilagyi, J. (2002). Vegetation indices to aid areal evapotranspiration estimations. *Journal of Hydrologic Engineering, 7*, 368−372.

Tanner, C. B., & Jury, W. A. (1976). Estimating evaporation and transpiration from a row crop during incomplete cover. *Agronomy Journa, 68*, 239−242.

Tuzet, A., Perrier, A., & Leuning, R. (2003). A coupled model of stomatal conductance, photosynthesis and transpiration. *Plant, Cell and Environment, 26*, 1097−1116.

Twine, T. E., Kustas, W. P., Norman, J. M., Cook, D. R., Houser, P. R., Meyers, T. P., et al. (2000). Correcting eddy-covariance flux underestimates over a grassland. *Agricultural and Forest Meteorology, 103*, 279−300.

Welles, J. M., & Norman, J. M. (1991). Instrument for indirect measurement of canopy architecture. *Agronomy Journal, 83*, 818−825.

Wong, S. C., Cowan, I. R., & Farquhar, G. D. (1979). Stomatal conductance correlates with photosynthetic capacity. *Nature, 282*, 424−426.

Zhan, X., & Kustas, W. P. (2001). A coupled model of land surface CO2 and energy fluxes using remote sensing data. *Agricultural and Forest Meteorology, 107*, 131−152.